Continuum model to define the chemistry and mass transfer in a bicarbonate electrolyzer

Eric W. Lees,[1,2] Justin C. Bui,[3,4] Datong Song,[5] Adam Z. Weber,*[2,4] and Curtis P. Berlinguette*[1,6,7,8]

[1]Department of Chemical and Biological Engineering, The University of British Columbia, 2360 East Mall, Vancouver, British Columbia, V6T 1Z3, Canada.

[2]Energy Technologies Area, Lawrence Berkeley National Laboratory, Berkeley, CA 94720, USA.

[3]Department of Chemical and Biomolecular Engineering, University of California, Berkeley, Berkeley, CA 94720, USA

[4]Liquid Sunlight Alliance, Lawrence Berkeley National Laboratory, Berkeley, CA 94720, USA.

[5]Energy, Mining and Environment Research Centre, National Research Council Canada, Vancouver, B.C. V6T 1W5, Canada.

[6]Department of Chemistry, The University of British Columbia, 2036 Main Mall, Vancouver, British Columbia, V6T 1Z1, Canada.

[7]Stewart Blusson Quantum Matter Institute, The University of British Columbia, 2355 East Mall, Vancouver, British Columbia, V6T 1Z4, Canada.

[8]Canadian Institute for Advanced Research (CIFAR), 661 University Avenue, Toronto, M5G 1M1, Ontario, Canada.

*Corresponding authors: Adam Z. Weber (azweber@lbl.gov) and Curtis P. Berlinguette (cberling@chem.ubc.ca)

Abstract

Bicarbonate electrolyzers are devices designed to convert CO_2 captured from point sources or the atmosphere into chemicals and fuels without needing to first isolate pure CO_2 gas. We report here an experimentally-validated model that quantifies the reaction chemistry and mass transfer processes within the catalyst layer and cation exchange membrane layer of a bicarbonate electrolyzer. Our results demonstrate that two distinct chemical microenvironments are key to forming CO at high rates: an acidic membrane layer that promotes *in situ* CO_2 formation, and a basic catalyst layer that suppresses the hydrogen evolution reaction. We show that the rate of CO product formation can be increased by modulating the catalyst and membrane layer properties to increase the rate of *in situ* CO_2 generation and transport to the cathode. These insights serve to inform the design of bicarbonate and BPM-based CO_2 electrolyzers while demonstrating the value of modeling for resolving rate-determining processes in electrochemical systems.

CO_2 electrolyzers can produce carbon-neutral chemicals and fuels using CO_2 from the atmosphere and electricity from wind and solar resources.[1–3] To be industrially relevant, CO_2 electrolyzers must achieve high rates of product formation (i.e., current densities >100 mA cm^{-2}) and low cell potentials (<3 V) while also efficiently utilizing the CO_2 reactant.[4, 5] Gaseous CO_2 is often used as the feedstock for pilot-scale CO_2 electrolyzers because of its solubility and mass transfer advantages over CO_2 dissolved in water.[6–8] However, isolating pure CO_2 gas from point sources or the atmosphere is costly because a considerable energy penalty (e.g., 50–175 kJ mol^{-1} CO_2) is required to liberate CO_2 from liquid sorbents used in CO_2 capture processes.[9–12] These collected CO_2 streams are also not often utilized efficiently in gas-fed CO_2 electrolyzers[13–16,] since often a major fraction of the reacted CO_2 is converted into HCO_3^- and CO_3^{2-} [referred to here as (bi)carbonates] upon reacting with OH^- produced at the cathode.[16,17] These issues associated with poor utilization of captured CO_2 gas add cost and complexity when deploying a CO_2 electrolyzer at scale.[16,18,19]

As a means of addressing the above challenges, we recently demonstrated that HCO_3^- solutions (an intermediate in CO_2 capture processes) can be reduced into valuable products (e.g., CO) at high rates using a flow electrolyzer architecture (**Fig. 1a**).[20–22] The primary benefit of "bicarbonate electrolysis" is that it eliminates the need for CO_2 regeneration, gas handling and compression in upstream CO_2 capture (**Fig. S1**).[23,24] Central to this technology is a continuous supply of H^+ to the cathode, which serves to liberate CO_2 from the bicarbonate solution and provide the reactant for CO_2 reduction.[20,21] This method of using H^+ to generate CO_2 *in situ* eliminates the carbonation problem discussed above for alkaline CO_2 electrolyzers.[16,20] High yields for CO (i.e., 40–70%) have therefore been reported for bicarbonate electrolyzers,[21] and more generally for CO_2 electrolyzers that supply H^+ to the cathode.[25,26] Collectively, these features of bicarbonate electrolysis reduce the cost of integrating CO_2 reduction with CO_2 capture by intensifying the process.[23]

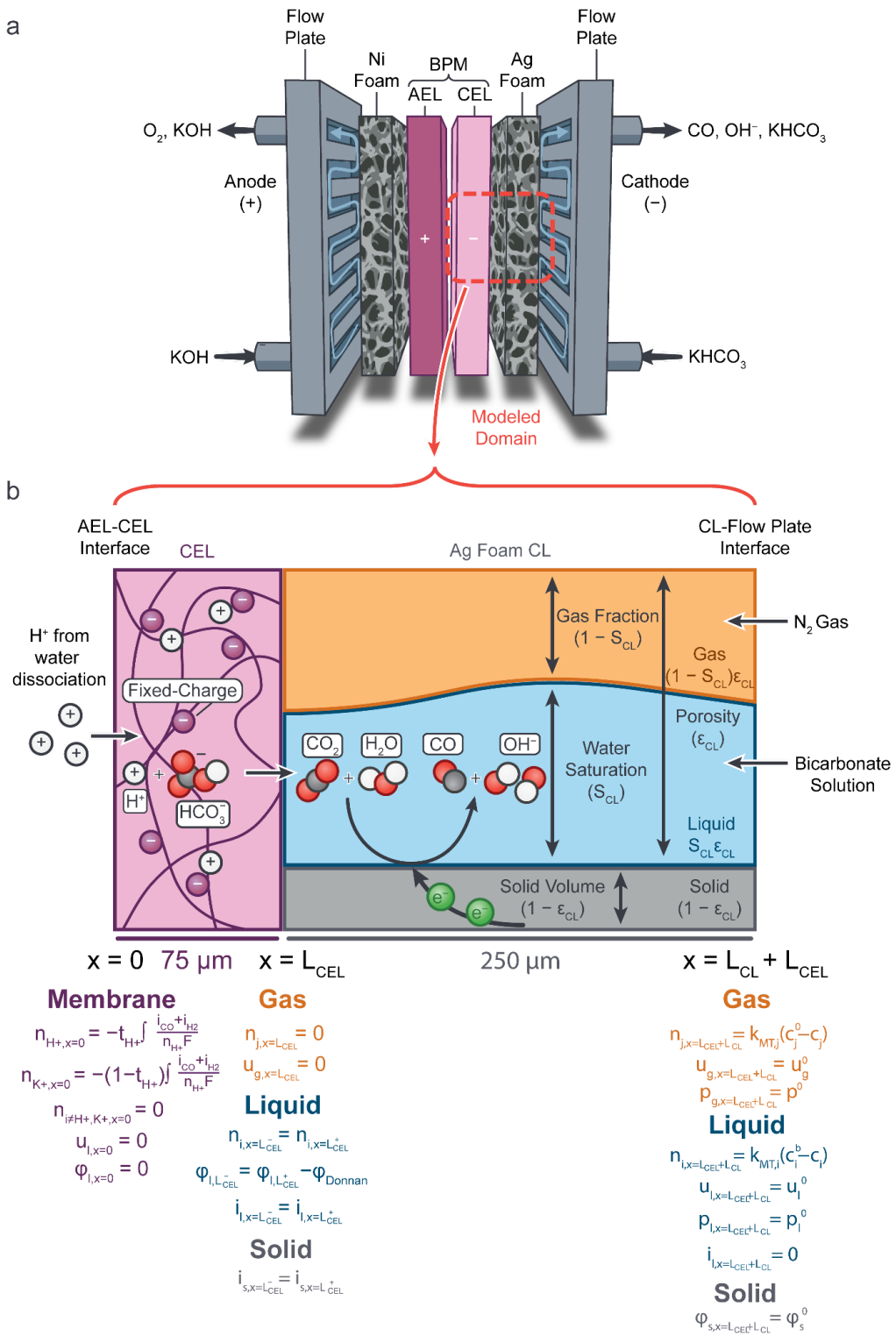

Figure 1: (a) Schematic diagram of a bicarbonate electrolyzer consisting of flow plates, a nickel foam anode, a BPM, and a silver foam cathode. The anode mediates OER and the BPM mediates water dissociation. Sequential reactions occur in the cathode: bicarbonate reacts with protons to form CO_2 *in situ*, which then is subsequently reduced to form CO and OH^-. (b) A representation of the cation exchange layer (CEL) and catalyst layer (CL) and phases (gas, liquid, and solid)

described by the continuum model. Boundary conditions are defined at the AEL/CEL interface ($x = 0$), CEL/CL interface ($x = L_{CEL}$), and at the CL/flow plate interface ($x = L_{CEL} + L_{CL}$).

This study investigates a bicarbonate electrolyzer architecture containing a nickel foam anode, a silver foam cathode, and a BPM (**Fig. 1a**).[20,27] The BPM consists of an anion exchange layer (AEL) and cation exchange layer (CEL) with a water-dissociation catalyst at their interface.[20,21,28] Under a reverse bias, water dissociation (**Eq. 1**) occurs at the AEL/CEL interface to supply OH^- to the anode for the oxygen evolution reaction (OER; **Eq. 2**)[29] and H^+ to the cathode where it reacts with (bi)carbonates to form CO_2 *in situ* (**Eqs. 3, 4**). The produced CO_2 is then electrochemically reduced into CO at the surface of a silver foam catalyst layer (CL) with OH^- produced as a byproduct (**Eq. 5**).[30] In an ideal scenario, these reactions would be perfectly selective and irreversible to enable high CO formation rates. However, several competitive reactions and parasitic processes reduce electrolyzer efficiencies. For example, the hydrogen evolution reaction (**Eq. 6**) competes with CO_2 reduction at the cathode. Furthermore, CO_2 that is formed *in situ* can react with electrochemically-generated OH^- to reform (bi)carbonates (**Eqs. 7, 8**) or remain unreacted in the cathodic product stream. The complex interplays and nonlinearities make it hard to easily understand and resolve the individual processes, and it is therefore challenging to navigate and select electrolyzer design parameters (i.e., material properties, reactor geometries, and operating conditions).

$$H_2O_{(l)} \rightleftharpoons OH^-_{(aq)} + H^+_{(aq)} \qquad K_w = 10^{-14} M^2 \qquad \textbf{Eq. 1}$$

$$2OH^-_{(aq)} \rightarrow 2e^- + \tfrac{1}{2}O_{2(g)} + H_2O_{(l)} \qquad E^0 = +0.41\ V \text{ vs. SHE}^{31} \qquad \textbf{Eq. 2}$$

$$HCO_3^-{}_{(aq)} + H^+_{(aq)} \rightleftharpoons CO_{2(aq)} + H_2O_{(l)} \qquad K_1 = 10^{-6.37} \qquad \textbf{Eq. 3}$$

$$HCO_3^-{}_{(aq)} \rightleftharpoons CO_3^{2-}{}_{(aq)} + H^+_{(aq)} \qquad K_2 = 10^{-10.32} M \qquad \textbf{Eq. 4}$$

$$CO_{2(aq)} + H_2O_{(l)} + 2e^- \rightarrow CO_{(g)} + 2OH^-_{(aq)} \qquad E^0 = -0.11\ V \text{ vs. SHE}^{32,33} \qquad \textbf{Eq. 5}$$

$$2H^+_{(aq)} + 2e^- \rightarrow H_{2(g)} \qquad E^0 = 0.00\ V \text{ vs. SHE} \qquad \textbf{Eq. 6}$$

$$CO_{2(aq)} + OH^-_{(aq)} \rightleftharpoons HCO_3^-{}_{(aq)} \qquad K_3 = \frac{K_1}{K_w} \qquad \textbf{Eq. 7}$$

$$HCO_3^-{}_{(aq)} + OH^-_{(aq)} \rightleftharpoons H_2O_{(l)} + CO_3^{2-}{}_{(aq)} \qquad K_4 = \frac{K_2}{K_w} \qquad \textbf{Eq. 8}$$

Multiphysics modeling is ideally suited to explore various physical phenomena relevant to CO_2 electrolysis and accelerate the design of optimal reactor architectures.[34] However, there are strikingly few CO_2 electrolyzer models, in part due to the numerical challenges associated with coupling highly non-linear transport equations with numerous acid-base and electrochemical reactions. CO_2 reduction models are therefore often developed with simplified reaction or mass transfer kinetics to reduce model complexity.[35–38] Recently, models have been developed that effectively simulate coupled reaction and mass transfer processes in CO_2 electrolyzers and generally agree with experimental results without the need for empirical parameter fitting.[32,33,39–42] Using volume-averaged approaches, continuum models can capture the interactions between electrochemistry, acid-base chemistry, and transport phenomena within CO_2 electrolyzers. Importantly, these types of models can inform how electrolyzer design and material properties affect the in-plane transport of ionic species,[32] failure mechanisms,[33] and CO_2 reduction product selectivity.[40] Notwithstanding, the majority of CO_2 reduction models have focused on devices that mediate CO_2 reduction at highly alkaline cathodes and therefore endure significant CO_2 losses to (bi)carbonate formation and transport.[32,40] The only demonstrated solution to these challenges of low-temperature CO_2 electrolysis is to use an electrolyzer that leverages one or more of the following: (i) a supply of H^+ to the cathode to neutralize (bi)carbonates[25,26] or (ii) a CO_2 capture medium as the carbon-bearing feedstock.[43–45] While these approaches appear to be the most promising way forward, no device-scale models have been developed that simulate the relevant physics in these architectures and compare the results to real experimental data.

We demonstrate here a continuum model for the cathode compartment of a bicarbonate electrolyzer which was validated with electrolyzer experiments (**Fig. 1b**). This model enabled investigation into fundamental relationships between the chemical environment (i.e., pH and CO_2 concentration) in the cathode and the activity and selectivity of CO formation. Importantly, our computational and experimental results demonstrate how H^+-mediated *in-situ* CO_2 generation improves CO_2 reduction product yields within an electrolyzer.[25,26] Model insights were used to elucidate membrane and electrode properties that improve performance parameters by modulating mass transport of chemical species within the electrolyzer. In sum, this study provides guidance into the design of future improved architectures based on elucidation of underlying phenomena of the chemical microenvironments.

Results and Discussion

The model was developed to predict bicarbonate electrolyzer performance using parameter values obtained from literature (**Table S1**). The 3-dimensional solid, liquid, and gas phases were represented as homogeneous, 1-dimensional continuums with volume-averaged values for key properties (e.g., porosity, tortuosity, active surface area, and water saturation). Mass transfer was modeled in the through-plane direction because previous reports have shown that the flow channel and porous CL of flow electrolyzers promote relatively uniform mixing in the in-plane direction.[40,41] The governing equations (based on mass, momentum, and charge conservation) were solved simultaneously to quantify the steady-state concentrations of liquid species (H^+, OH^-, K^+, CO_2, HCO_3^-, and CO_3^{2-}), gas species (CO_2, CO, and N_2) as well as the rates of the CO2RR (**Eq. 5**), HER (**Eq. 6**), and acid-base reactions (**Eqs. 3, 4 and 7, 8**). The boundary conditions are summarized in **Fig. 2b**.

The model was validated using a bicarbonate electrolyzer architecture that was previously demonstrated to enable high CO formation activity and stability.[73] This electrolyzer is composed of flow

plates, a nickel foam anode (~250 μm), a BPM, and a silver foam cathode. The silver foam cathode was fabricated by treating silver foam substrates with 30 % (v/v) nitric acid (**Fig. S2**).[73] Cross-sectional scanning electron microscopy (SEM) images were used to estimate the silver foam thickness as 250 μm (**Fig. S2b** and **Fig. S2d**). Top-view SEM images taken before (**Fig. S2a**) and after (**Fig. S2c**) electrolysis showed no obvious morphological differences.

Electrolysis experiments were performed at constant current densities of 50, 100, 200, and 300 mA cm^{-2} while solutions of 1 M KOH and 3 M $KHCO_3$ were delivered to the anodic and cathodic flow plates, respectively. Gaseous reaction products formed at the cathode were delivered to the sample loop of a gas chromatograph (GC) using a stream of N_2 gas that was swept through the headspace of the 3 M $KHCO_3$ reservoir. GC measurements were performed after 5 min of electrolysis to ensure the reaction products had reached saturation concentrations in the catholyte before analysis.[21] To determine if liquid products were produced, aliquots of the catholyte were collected after 20 min of electrolysis and analyzed using ^1H nuclear magnetic resonance spectroscopy. Each electrolysis experiment was performed in triplicate to determine the FE_{CO} error bars.

Model validation using experimental electrolysis data

The cathodic product stream of the electrolyzer consisted of CO, H_2, and CO_2, and no liquid CO_2 reduction products were detected. The FE_{CO} values decreased from 68 ± 5% to 35 ± 3% as the current density was incrementally increased from 50 to 300 mA cm^{-2} (**Fig. 2a**) and the experimental CO yields increased from 51 ± 8% to 74 ± 6% over the same current density range (**Fig. 2b**). These experimental results agreed remarkably well with the modeling results in terms of partial current densities (**Fig. S3**) and FE_{CO} values (**Fig. 2a**), especially when considering that the model parameters were obtained directly from literature and not fit to the collected experimental data. The model also predicted the experimental

CO yields within experimental error at current densities ranging from 50 to 200 mA cm^{-2} (**Fig. 2b**). However, the predicted and experimental values diverged at 300 mA cm^{-2}. At this high current density, a high rate of OH^- formation increased the pH of the electrolyte in the reservoir (from ~8.5 to ~9), thereby causing an increase in CO_2 conversion to carbonate as the equilibrium shifted towards CO_3^{2-} over the course of the experiment (**Fig. S4**).[20] The model does not account for this higher pH at the CL/flow plate interface and instead uses a constant bulk electrolyte composition (with a pH of 8.5; **Table S2**)[52] in the mass-flux boundary condition (**Fig. 1b**). We believe this simplification in the model framework is causing the model to underpredict the experimental CO yields. Nonetheless, the simulation exhibits good agreement with the experimental data over a wide range of applied current densities. A higher-dimensional model that accounts for the equilibrium in the flow channel and electrolyte reservoir is needed to predict these values more accurately, but this is beyond the scope of the current work.

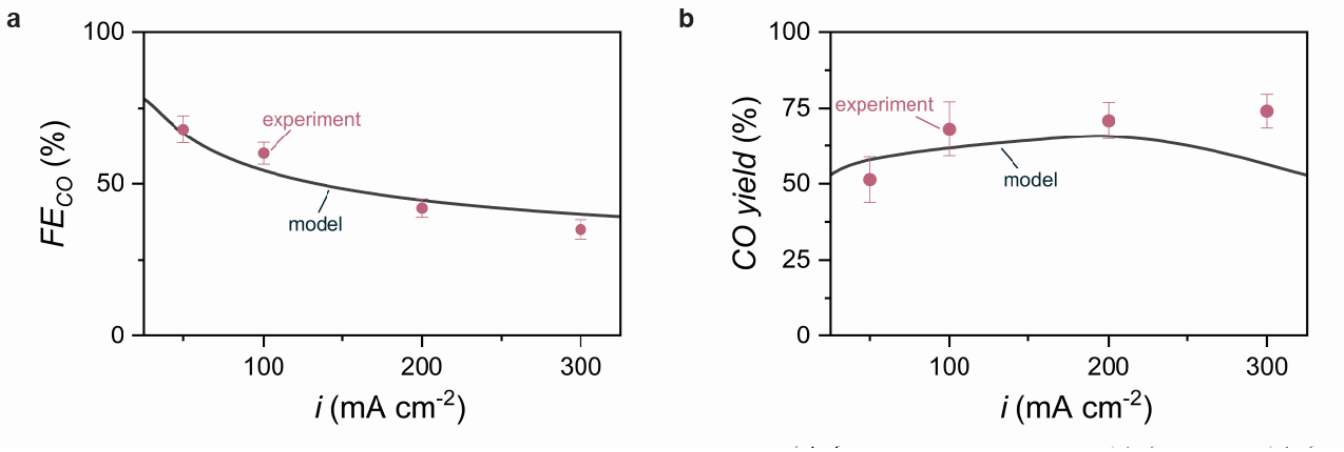

Figure 2: Experimental validation of the cathode model for bicarbonate electrolysis. (a) Experimental (purple circles) and modeled (black lines) data for the (a) FE_{CO} and (b) CO yields as a function of current density. Note that the model was developed using parameters obtained directly from literature without using additional fitting parameters to match the experimental data.

Generation and transport of CO_2

The validated model enables one to investigate the cause for the observed decrease in FE_{CO} values observed at high current densities. We conjectured that the reaction is limited by CO_2 mass transfer and therefore we used the model to track CO_2 generation from bicarbonate and conversion of CO_2 into CO. The model results show that water dissociation within the BPM produces an H^+ flux that decreases the pH decreases towards the AEL/CEL interface (i.e., at $x = 0$) (**Fig. 3a**). The modeled CO_2 concentration increases within the CEL (**Fig. 3b**) because (bi)carbonates are converted into CO_2 in acidic conditions (**Eq. 3, 4**). As the current density is increased, a proportional increase in the H^+ flux from the AEL/CEL interface enhances the rate of *in situ* CO_2 generation. Consequently, CO_2 bubbles can be observed nucleating at the CEL/electrolyte interface during electrolysis experiments.[20] CO_2 that is produced through this pathway is subsequently reduced or reacted in the CL (**Eq. 5** and **Eq. 8-9**, respectively). These CO_2 consumption processes decrease the steady-state concentrations of CO_2 to < 1 mM throughout the majority of the CL. These results, combined with the experimental observations of decreased FE_{CO} at high current densities, indicate that CO_2 mass transport limits the rate of CO formation in the system.

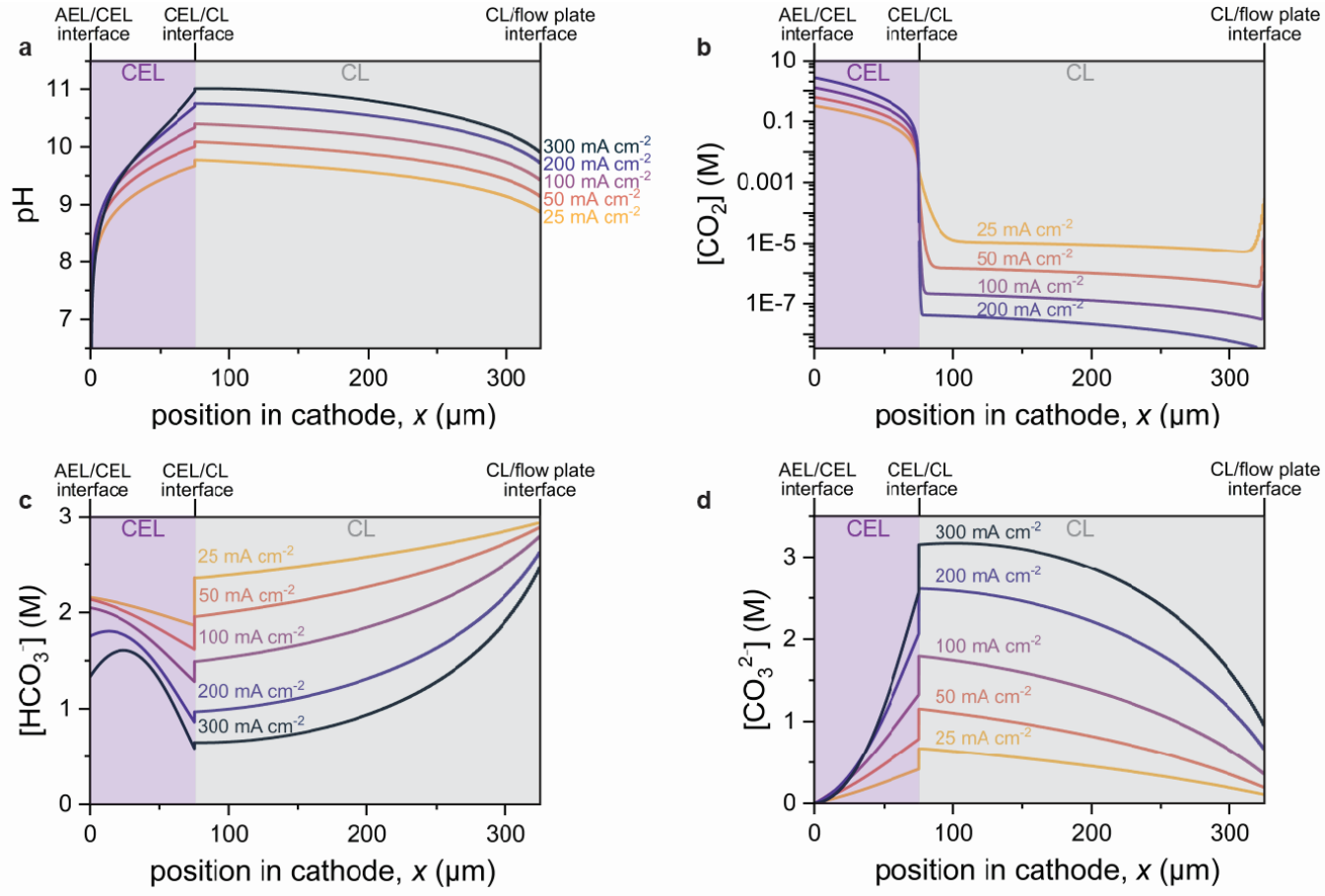

***Figure 3**:* Modeled (a) pH (b) CO_2 (c) HCO_3^- and (d) CO_3^{2-} concentrations within the bicarbonate electrolyzer cathode for different applied current densities. Shaded regions indicate the location of the CEL (purple; $x = 0$ *to* 75 μm) and CL (grey; $x = 75$ *to* 325 μm).

The model demonstrates that the competitive CO_2 generation and consumption processes in the CEL and CL, respectively, cause CO_2 concentration gradients (**Fig. 3b**) at the CEL/CL interface. These concentration gradients at the CEL/CL interface give rise to CO_2 fluxes of 1.1, 1.8, 2.8, 3.9, and 5.3 mmol m^{-2} s^{-1} towards the CL for current densities of 25, 50, 100, 200, and 300 mA cm^{-2}, respectively (**Fig. S5a**). These fluxes constitute the majority of the corresponding modeled CO formation rates (1.0, 1.7, 2.8, 4.6, and 6.2 mmol m^{-2} s^{-1} at the same respective current densities). Consequently, the modeled CO_2 concentration profiles in the CL (**Fig. S5b**) and CO formation rates (**Fig. S5c**) are higher near the CEL/CL interface than the rest of the CL. Collectively, these results suggest that regions of the CL closer to the CEL should be more active for CO formation. This conjecture is supported by previous

experiments, which showed that the silver catalyst layers near the BPM had a more significant impact on CO formation rates than the silver catalyst layers added to the backside of the electrode (at the CL/flow plate interface).[21]

The simulated (bi)carbonates concentration profiles are consistent with the modeled pH and CO_2 concentration profiles in terms of the chemical equilibrium (**Fig S4**). As the current density increases, the HCO_3^- concentration in the CEL decreases (**Fig. 3c**) because HCO_3^- reacts with H^+ from water dissociation to form CO_2. In the CL, the HCO_3^- concentration decreases as the current density increases because electrochemically generated OH^- reacts with HCO_3^- to form CO_3^{2-}. This reaction stoichiometry is also reflected in the modeled CO_3^{2-} concentration profiles in the CL, which increase with increasing current density (**Fig. 3d**). Both the HCO_3^- and CO_3^{2-} concentration profiles exhibit a discontinuity at the CEL/CL interface because of Donnan exclusion (i.e., the fixed negative charges in the CEL repel the negatively-charged HCO_3^- and CO_3^{2-}; **Eq. S7**).[48] The corresponding electrolyte potential and K^+ concentration profiles are shown in **Fig. S6**.

These modeling results provide insight into how the dynamic pH-dependent reactions between (bi)carbonates and CO_2 enable CO formation. The HCO_3^-/CO_2 equilibrium reaction (pKa = 6.31) enables HCO_3^- to convert rapidly into CO_2 in the relatively acidic environment within the CEL. At the same time, the HCO_3^-/CO_3^- equilibrium reaction (pKa = 10.32) enables the pH to rise rapidly within the CL. The high pH in the CL serves to suppress hydrogen evolution, and therefore, enable higher CO product formation rates. These disparate microenvironments in the CEL and CL are essential to a H^+ flux-mediated CO_2 generation mechanism.[25,26]

Impact of H^+ flux and bulk pH on CO formation rates

Without a H^+ flux to the cathode, the only source of CO_2 in a bicarbonate electrolyzer is the bulk electrolyte, which has a CO_2 concentration of ~8 mM according to the chemical equilibrium.[52] We modeled how much CO can be formed exclusively from this source of CO_2 by removing the water-dissociation boundary condition at the AEL/CEL interface. Specifically, we reduced the fraction of ionic current associated with H^+ transport (i.e., the transference number of H^+, t_{H+}) at the AEL/CEL interface from 0.9 to 0 (**Eq. S5**) while increasing the transference number of K^+ (t_{K+}) from 0.1 to 1 (**Eq. S6**). The model results exhibited higher cathodic pH values (**Fig. 4a**) and lower corresponding CO_2 generation rates without the H^+ flux. Accordingly, lower FE_{CO} values were observed (**Fig. 4b**). These modeling results are consistent with our previously-reported experimental data which showed that replacing the BPM with an anion exchange membrane results in lower CO formation rates.[20]

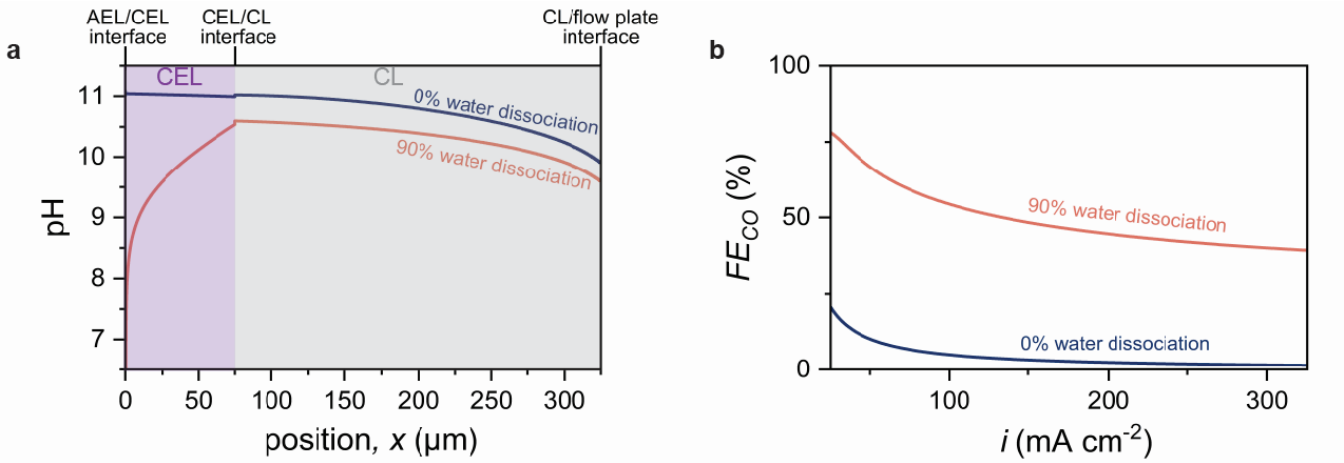

***Figure 4**:* (a) pH profiles and (b) FE_{CO} values for water dissociation rates equal to 0 and 90% of the total charge transport in the liquid phase at the AEL/CEL interface when a total current density of 150 mA cm^{-2} is applied. The different water dissociation rates were modeled by toggling the t_{H+} and t_{K+} values at the AEL/CEL interface (**Eq. 13** and **Eq. 14**).

The bulk pH of the CO_2 capture solution feedstock is an important parameter for bicarbonate electrolysis because it defines the equilibrium concentrations of CO_2, HCO_3^-, and CO_3^{2-} in the flow plate (**Fig. S4**). The impact of this parameter on CO formation was investigated by modulating the bulk

electrolyte concentrations (**Table S2**) in the mass flux boundary conditions at the CL/flow plate interface (**Eq. S39**). A pH regime between 8.5 and 10 was selected to reflect the composition of CO_2 capture solutions used in industry.[74–76] The modeling results show that increasing the bulk pH generally decreases the FE_{CO} (**Fig. S7**). A more pronounced effect is observed at low current densities (i.e., <100 mA cm^{-2}) because a lower associated H^+ flux from water dissociation reduces the rate of *in situ* CO_2 generation. At these low current densities, the CO_2 in the bulk electrolyte serves as a primary source of CO_2 for CO_2 reduction.[52,77,78] Low CO formation rates are therefore observed with higher pH solutions that have lower bulk CO_2 concentrations (**Table S2**). However, at current densities >100 mA cm^{-2}, the supply of CO_2 from H^+-mediated CO_2 generation increases and therefore the effect of bulk CO_2 concentration has a less pronounced effect on FE_{CO} (**Fig. S5a**). Notwithstanding, higher pH feedstocks yield lower CO formation rates, even at high current densities, because CO_2 generation from CO_3^{2-} requires twice the H^+ supply as HCO_3^- according to the stoichiometry (**Eq. 3, 4**).

CEL and CL properties predicted by modeling

A primary purpose of developing the model is elucidation and subsequent mitigation of the rate-limiting step that gates CO formation. Our experimental and computational results confirm that CO_2 mass action is limiting because the concentration of CO_2 in the CL is depleted at high current densities (**Fig. 3c**). We therefore computationally investigated CEL and CL material properties that could be independently modulated to increase CO_2 mass transport in order to access higher CO formation rates.

Water dissociation in the BPM provides the H^+ necessary to generate electrochemically-active CO_2 (**Fig. 4**). From an experimental perspective, the H^+ flux from water dissociation can be increased by using: (i) an improved water dissociation catalyst;[59] or (ii) a CEL material composed of an ionomer with a higher concentration of fixed-charge groups [i.e., a higher ion exchange capacity (IEC)] that amplifies

the electric field and hence charge repulsion at the AEL/CEL interface.[48,61,79] As described earlier, the effect of (i) on the FE_{CO} was investigated by increasing t_{H+} (**Eq. S5**) at the AEL/CEL interface, and the modeled FE_{CO} values increased as expected (**Fig. S8a**). Increased water dissociation activity results in a lower pH near the AEL/CEL interface (**Fig. S8b**) which increases *in situ* CO_2 formation (**Fig. S8c**). To investigate (ii), the ionomer IEC was increased from 1 to 3 mmol g^{-1}. The FE_{CO} increased due to inhibited OH^- transport at the CL/CEL interface, which caused a pH increase in the CL (**Fig. S8d**). Therefore, the positive effect of a higher IEC ionomer on FE_{CO} values is two-fold: it decreases the pH in the CEL by enhancing water dissociation and it increases the pH in the CL to suppress hydrogen evolution.

The residence time of H^+ in the CEL impacts the local pH environments in the cathode, which, in turn, determines the kinetics of *in situ* CO_2 generation and reduction. To quantify the impact of H^+ residence time on bicarbonate electrolysis, three CEL thicknesses (25, 50, and 75 μm) were simulated and the FE_{CO} values were compared at a constant current density of 150 mA cm^{-2} (**Fig. S9**). The results show that increasing CEL thickness increases the FE_{CO} by modulating ion transport (**Fig. S9a**). Thicker CELs were found to elongate the H^+ diffusion path from the AEL/CEL interface to the CEL/CL interface. Consequently, thicker CELs gave rise to higher pH values in the CL because of slower H^+ transport to the CL (**Fig. S9b**). These synergistic pH effects enable higher CO_2 concentrations in the CEL (**Fig. S9c**) and diminished hydrogen evolution in the CL. It is for these reasons that thicker CELs are predicted to achieve higher CO formation rates than thinner CELs. However, thicker CELs increase ohmic resistance (**Fig. S9d**), and therefore, electrolyzer energy consumption.

The impact of CL thickness and porosity on FE_{CO} was simulated to determine the effect of mass transport rates on the FE_{CO}.[80,81] The results show that decreasing the CL thickness from 250 to 50 μm increases the FE_{CO} from 48 to 79% at 150 mA cm^{-2} (**Fig. S10a**), which may explain why thinner silver catalyst layers (<10 μm) have enabled FE_{CO} values of ~80% in previous bicarbonate electrolysis

studies.[21] One of the drivers for this increased performance is the higher concentration of CO_2 in the CEL when using a thin catalyst layer (**Fig. S10b**). This improvement in *in situ* CO_2 generation is due to a shorter diffusion path for (bi)carbonates to transport from the flowplate through the CL to the H^+ source in the CEL. Higher HCO_3^- concentrations are therefore observed in thinner CLs because of faster HCO_3^- mass transfer towards the CEL (**Fig. S10c**). Similar to the effect of decreasing CL thickness, increasing CL porosity increases the rate at which (bi)carbonates transport to the CEL (**Fig. S10d**). As above, a faster mass transport rate of (bi)carbonates to the CEL results in more CO_2 formation (**Fig S10e**), which increases the rate of CO_2 reduction (**Fig S10f**). While these results are readily rationalized, it should be noted that a more detailed model which captures flow channel and 3D effects is needed to characterize these parameters fully.[38,82,83]

Considering the above property-performance relationships, **Fig. 5** shows the cumulative impact of the "improved case" compared to the "basecase". The improved parameters yield a significant increase in FE_{CO} relative to the basecase across the range of simulated current densities. These observations are a result of elevated CO_2 concentrations in the CEL (**Fig. 5b**), and consequently the CO_2 flux to the CL (**Fig. S11**). As discussed above, the additive and potentially synergistic effects of these improved material properties enables: (i) efficient mass transport through the thin, porous CL; (ii) prolonged residence time for reactive species in the CEL; (iii) suppression of hydrogen evolution in the CL; and (iv) a higher H^+ concentration in the CEL. The model results serve as benchmarks for future experimental studies to improve the performance of this device and other CO_2 electrolyzers that utilize H^+-mediated CO_2 generation at the cathode.[26]

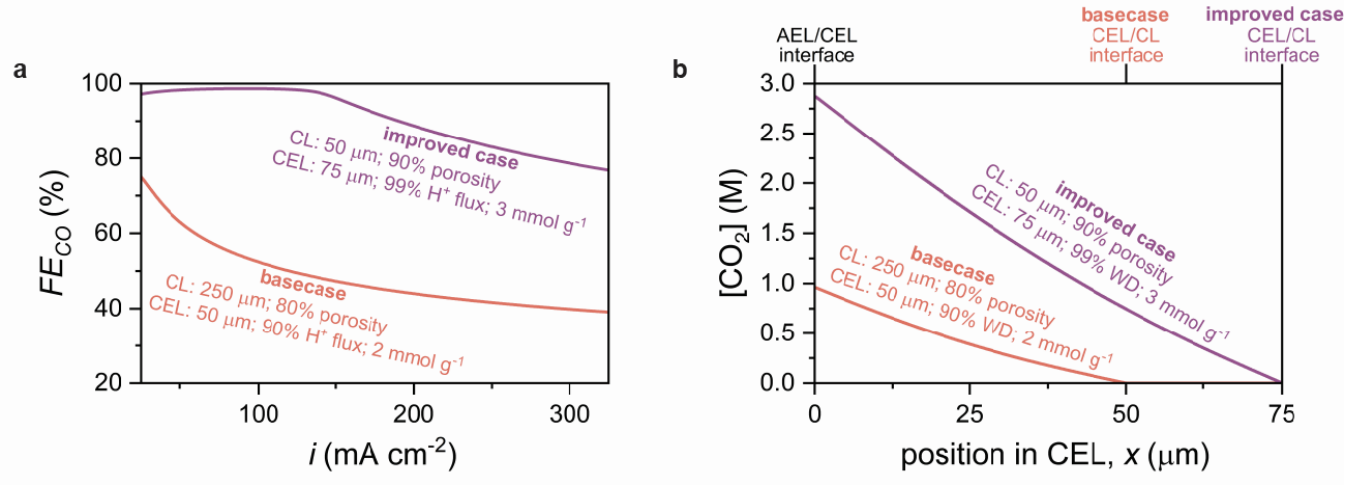

***Figure 5**:* (a) Modeled FE_{CO} values as a function of current density for the improved CEL and CL properties (99% H^+ flux; CEL thickness = 75 μm; IEC = 3 mmol g^{-1}; CL porosity = 0.9; CL thickness = 50 μm) and the basecase properties (90% H^+ flux; CEL thickness = 50 μm; IEC = 2 mmol g^{-1}; CL porosity = 0.8; CL thickness = 250 μm). (b) CO_2 concentration profiles in the CEL for the improved case and the basecase at a constant current density of 150 mA cm^{-2}.

Conclusions

We report here an experimentally-validated continuum model for the cathode of a bicarbonate electrolyzer. The model was used to investigate the *in situ* CO_2 generation and reduction mechanism, which eliminates carbonation issues in CO_2 electrolyzers and enables high CO formation rates (>100 mA cm^{-2}) from bicarbonate solutions. The results demonstrate the existence of two disparate pH microenvironments associated with this mechanism: an acidic electrolyte/membrane region where H^+ reacts with HCO_3^- to form CO_2, and an alkaline catalyst layer region that reduces CO_2 to CO and suppresses the competitive hydrogen evolution reaction. A low CO_2 concentration in the catalyst layer slows CO_2 reduction at high current densities, and this mass transfer limitation can be overcome by optimizing material properties. Several model parameters were identified as levers for increasing CO_2 supply rates to the catalyst layer: the rate of water dissociation, the ion exchange capacity and thickness of the membrane, and the thickness and porosity of the catalyst layer. Through modeling and quantifying

the complex pH and CO_2 gradients in CO_2 reduction electrolyzers, one can derive a deeper understanding and help guide the development of materials with enhanced performance.

Acknowledgements

The authors thank Dr. Zishuai Zhang and Alyssa Liu for help with performing electrolysis experiments and David Dvorak for SEM imaging. The authors are grateful to the Canadian Natural Science and Engineering Research Council (CRDPJ 536621 - 18), the National Research Council of Canada's Materials for Clean Fuels Challenge Program (MCF-107), Canadian Foundation for Innovation (229288), Canadian Institute for Advanced Research (BSE-BERL-162173), TOTAL American Services, Inc (an affiliate of TotalEnergies SE, France), and the Canada Research Chairs for financial support. SEM imaging was performed in the Centre for High-Throughput Phenogenomics at the University of British Columbia, a facility supported by the Canada Foundation for Innovation, British Columbia Knowledge Development Foundation, and the UBC Faculty of Dentistry. This research was undertaken thanks in part to funding from the Canada First Research Excellence Fund, Quantum Materials and Future Technologies Program. This material is also based on work performed by the Liquid Sunlight Alliance, which is supported by the U.S. Department of Energy, Office of Science, Office of Basic Energy Sciences, Fuels from Sunlight Hub under Award Number DE-SC0021266. E.W.L. acknowledges funding from National Science and Engineering Research Council (NSERC) and Killam Doctoral Fellowships. J.C.B acknowledges funding from the National Science Foundation Graduate Research Fellowship under Grant No. DGE 1752814.

Conflicts of Interest

Authors CPB and EWL have filed a patent application for the technology analyzed in this work (U.S. application No. 62/662,391).

Supporting Information

Materials and methods and supplementary data can be found in the Supporting Information

References

(1) Hori, Y.; Kikuchi, K.; Suzuki, S. PRODUCTION OF CO AND CH4 IN ELECTROCHEMICAL REDUCTION OF CO2 AT METAL ELECTRODES IN AQUEOUS HYDROGENCARBONATE SOLUTION. *Chem. Lett.* **1985**, *14* (11), 1695–1698.

(2) Hori, Y.; Murata, A.; Kikuchi, K.; Suzuki, S. Electrochemical Reduction of Carbon Dioxides to Carbon Monoxide at a Gold Electrode in Aqueous Potassium Hydrogen Carbonate. *J. Chem. Soc. Chem. Commun.* **1987**, *0* (10), 728–729.

(3) Hori, Y.; Kikuchi, K.; Murata, A.; Suzuki, S. PRODUCTION OF METHANE AND ETHYLENE IN ELECTROCHEMICAL REDUCTION OF CARBON DIOXIDE AT COPPER ELECTRODE IN AQUEOUS HYDROGENCARBONATE SOLUTION. *Chem. Lett.* **1986**, *15* (6), 897–898.

(4) Verma, S.; Lu, S.; Kenis, P. J. A. Co-Electrolysis of CO2 and Glycerol as a Pathway to Carbon Chemicals with Improved Technoeconomics due to Low Electricity Consumption. *Nature Energy* **2019**, *4* (6), 466–474.

(5) Jouny, M.; Luc, W.; Jiao, F. General Techno-Economic Analysis of CO_2 Electrolysis Systems. *Ind. Eng. Chem. Res.* **2018**, *57* (6), 2165–2177.

(6) Weekes, D. M.; Salvatore, D. A.; Reyes, A.; Huang, A.; Berlinguette, C. P. Electrolytic CO_2 Reduction in a Flow Cell. *Acc. Chem. Res.* **2018**, *51* (4), 910–918.

(7) Goldman, M.; Lees, E. W.; Prieto, P. L.; Mowbray, B. A. W.; Weekes, D. M.; Reyes, A.; Li, T.; Salvatore, D. A.; Smith, W. A.; Berlinguette, C. P. Chapter 10:Electrochemical Reactors. In *Carbon Dioxide Electrochemistry*; 2020; pp 408–432.

(8) Salvatore, D. A.; Weekes, D. M.; He, J.; Dettelbach, K. E.; Li, Y. C.; Mallouk, T. E.; Berlinguette, C. P. Electrolysis of Gaseous CO2 to CO in a Flow Cell with a Bipolar Membrane. *ACS Energy Lett.* **2018**, *3* (1), 149–154.

(9) Keith, D. W.; Holmes, G.; St. Angelo, D.; Heidel, K. A Process for Capturing CO2 from the Atmosphere. *Joule* **2018**, *2* (8), 1573–1594.

(10) van Straelen, J.; Geuzebroek, F. The Thermodynamic Minimum Regeneration Energy Required for Post-Combustion CO2 Capture. *Energy Procedia* **2011**, *4*, 1500–1507.

(11) Rochelle, G. T. Amine Scrubbing for CO2 Capture. *Science* **2009**, *325* (5948), 1652–1654.

(12) Wang, C.; Jiang, K.; Jones, T. W.; Yang, S.; Yu, H.; Feron, P.; Li, K. Electrowinning-Coupled CO2 Capture with Energy-Efficient Absorbent Regeneration: Towards Practical Application. *Chem. Eng. J.* **2021**, 131981.

(13) Ripatti, D. S.; Veltman, T. R.; Kanan, M. W. Carbon Monoxide Gas Diffusion Electrolysis That Produces Concentrated C2 Products with High Single-Pass Conversion. *Joule*. 2019, pp 240–256. https://doi.org/10.1016/j.joule.2018.10.007.

(14) Bhargava, S. S.; Proietto, F.; Azmoodeh, D.; Cofell, E. R.; Henckel, D. A.; Verma, S.; Brooks, C. J.; Gewirth, A. A.; Kenis, P. System Design Rules for Intensifying the Electrochemical Reduction of CO2 to CO on Ag Nanoparticles. *ChemElectroChem* **2020**. https://doi.org/10.1002/celc.202000089.

(15) Jeng, E.; Jiao, F. Investigation of CO2 Single-Pass Conversion in a Flow Electrolyzer. *React. Chem. Eng.* **2020**, *5* (9), 1768–1775.

(16) Rabinowitz, J. A.; Kanan, M. W. The Future of Low-Temperature Carbon Dioxide Electrolysis Depends on Solving One Basic Problem. *Nat. Commun.* **2020**, *11* (1), 5231.

(17) Lees, E. W.; Mowbray, B. A. W.; Parlane, F. G.; Berlinguette, C. P. Gas Diffusion Electrodes and Membranes for CO_2 Reduction Electrolyzers. *Nature Reviews Materials* **2021**.

(18) Sisler, J.; Khan, S.; Ip, A. H.; Schreiber, M. W.; Jaffer, S. A.; Bobicki, E. R.; Dinh, C.-T.; Sargent,

E. H. Ethylene Electrosynthesis: A Comparative Techno-Economic Analysis of Alkaline vs Membrane Electrode Assembly vs CO2–CO–C2H4 Tandems. *ACS Energy Lett.* **2021**, *6* (3), 997–1002.
(19) Jouny, M.; Hutchings, G. S.; Jiao, F. Carbon Monoxide Electroreduction as an Emerging Platform for Carbon Utilization. *Nature Catalysis* **2019**, *2* (12), 1062–1070.
(20) Li, T.; Lees, E. W.; Goldman, M.; Salvatore, D. A.; Weekes, D. M.; Berlinguette, C. P. Electrolytic Conversion of Bicarbonate into CO in a Flow Cell. *Joule* **2019**, *3* (6), 1487–1497.
(21) Lees, E. W.; Goldman, M.; Fink, A. G.; Dvorak, D. J.; Salvatore, D. A.; Zhang, Z.; Loo, N. W. X.; Berlinguette, C. P. Electrodes Designed for Converting Bicarbonate into CO. *ACS Energy Lett.* **2020**, *5* (7), 2165–2173.
(22) Li, T.; Lees, E. W.; Zhang, Z.; Berlinguette, C. P. Conversion of Bicarbonate to Formate in an Electrochemical Flow Reactor. *ACS Energy Lett.* **2020**, *5* (8), 2624–2630.
(23) Welch, A. J.; Dunn, E.; DuChene, J. S.; Atwater, H. A. Bicarbonate or Carbonate Processes for Coupling Carbon Dioxide Capture and Electrochemical Conversion. *ACS Energy Lett.* **2020**, *5* (3), 940–945.
(24) Crabtree, R. H. Alternate Strategies for Solar Fuels from Carbon Dioxide. *ACS Energy Lett.* **2020**, *5* (8), 2505–2507.
(25) Huang, J. E.; Li, F.; Ozden, A.; Sedighian Rasouli, A.; García de Arquer, F. P.; Liu, S.; Zhang, S.; Luo, M.; Wang, X.; Lum, Y.; Xu, Y.; Bertens, K.; Miao, R. K.; Dinh, C.-T.; Sinton, D.; Sargent, E. H. CO2 Electrolysis to Multicarbon Products in Strong Acid. *Science* **2021**, *372* (6546), 1074–1078.
(26) O'Brien, C. P.; Miao, R. K.; Liu, S.; Xu, Y.; Lee, G.; Robb, A.; Huang, J. E.; Xie, K.; Bertens, K.; Gabardo, C. M.; Edwards, J. P.; Dinh, C.-T.; Sargent, E. H.; Sinton, D. Single Pass CO2 Conversion Exceeding 85% in the Electrosynthesis of Multicarbon Products via Local CO2 Regeneration. *ACS Energy Lett.* **2021**, 2952–2959.
(27) Zhang, Z.; Lees, E. W.; Habibzadeh, F.; Salvatore, D. A.; Ren, S.; Simpson, G.; Wheeler, D. G.; Liu, A.; Berlinguette, C. P. Metallic Porous Electrodes Enable Efficient Bicarbonate Electrolysis. *ChemRxiv*, 2021. https://doi.org/10.26434/chemrxiv.12891071.v3.
(28) Zhang, Z.; Lees, E. W.; Ren, S.; Huang, A.; Berlinguette, C. P. Electrolytic Conversion of Bicarbonate Solutions to CO at >500 mA Cm^{-2} and 2.2 V. *ChemRxiv. Prepr.* **2021**.
(29) Luo, J.; Vermaas, D. A.; Bi, D.; Hagfeldt, A.; Smith, W. A.; Grätzel, M. Bipolar Membrane-Assisted Solar Water Splitting in Optimal pH. *Advanced Energy Materials* **2016**, *6* (13), 1600100.
(30) Lees, E. W.; Mowbray, B. A. W.; Salvatore, D. A.; Simpson, G. L.; Dvorak, D. J.; Ren, S.; Chau, J.; Milton, K. L.; Berlinguette, C. P. Linking Gas Diffusion Electrode Composition to CO_2 Reduction in a Flow Cell. *J. Mater. Chem. A.* **2020**, *8* (37), 19493–19501.
(31) Haynes, W. M. *CRC Handbook of Chemistry and Physics, 91st Edition*; Taylor & Francis Group, 2010.
(32) Weng, L.-C.; Bell, A. T.; Weber, A. Z. Towards Membrane-Electrode Assembly Systems for CO 2 Reduction: A Modeling Study. *Energy Environ. Sci.* **2019**, *12* (6), 1950–1968.
(33) Weng, L.-C.; Bell, A. T.; Weber, A. Z. Modeling Gas-Diffusion Electrodes for CO_2 Reduction. *Phys. Chem. Chem. Phys.* **2018**, *20* (25), 16973–16984.
(34) Corral, D.; Feaster, J. T.; Sobhani, S.; DeOtte, J. R.; Lee, D. U.; Wong, A. A.; Hamilton, J.; Beck, V. A.; Sarkar, A.; Hahn, C.; Others. Advanced Manufacturing for Electrosynthesis of Fuels and Chemicals from CO 2. *Energy Environ. Sci.* **2021**.
(35) Wheeler, D. G.; Mowbray, B. A. W.; Reyes, A.; Habibzadeh, F.; He, J.; Berlinguette, C. P. Quantification of Water Transport in a CO 2 Electrolyzer. *Energy Environ. Sci.* **2020**, *13* (12), 5126–5134.

(36) Burdyny, T.; Smith, W. A. CO2 Reduction on Gas-Diffusion Electrodes and Why Catalytic Performance Must Be Assessed at Commercially-Relevant Conditions. *Energy & Environmental Science*. 2019, pp 1442–1453. https://doi.org/10.1039/c8ee03134g.
(37) Delacourt, C.; Ridgway, P. L.; Kerr, J. B.; Newman, J. Design of an Electrochemical Cell Making Syngas (CO+ H_2)from CO_2 and H_2O Reduction at Room Temperature. *J. Electrochem. Soc.* **2008**, *155* (1), B42–B49.
(38) Bohra, D.; Chaudhry, J.; Burdyny, T.; Pidko, E.; Smith, W. Mass Transport in Catalytic Pores of GDE-Based CO2 Electroreduction Systems. *ChemRxiv*, 2020. https://doi.org/10.26434/chemrxiv.13073348.v1.
(39) Yang, Z.; Li, D.; Xing, L.; Xiang, H.; Xuan, J.; Cheng, S.; Yu, E. H.; Yang, A. Modeling and Upscaling Analysis of Gas Diffusion Electrode-Based Electrochemical Carbon Dioxide Reduction Systems. *ACS Sustainable Chem. Eng.* **2021**, *9* (1), 351–361.
(40) Weng, L.-C.; Bell, A. T.; Weber, A. Z. A Systematic Analysis of Cu-Based Membrane-Electrode Assemblies for CO 2 Reduction through Multiphysics Simulation. *Energy Environ. Sci.* **2020**, *13* (10), 3592–3606.
(41) Chen, Y.; Lewis, N. S.; Xiang, C. Modeling the Performance of A Flow-Through Gas Diffusion Electrode for Electrochemical Reduction of CO or CO2. *J. Electrochem. Soc.* **2020**, *167* (11), 114503.
(42) Bui, J. C.; Kim, C.; Weber, A. Z.; Bell, A. T. Dynamic Boundary Layer Simulation of Pulsed CO2 Electrolysis on a Copper Catalyst. *ACS Energy Lett.* **2021**, *6* (4), 1181–1188.
(43) Chen, L.; Li, F.; Zhang, Y.; Bentley, C. L.; Horne, M.; Bond, A. M.; Zhang, J. Electrochemical Reduction of Carbon Dioxide in a Monoethanolamine Capture Medium. *ChemSusChem* **2017**, *10* (20), 4109–4118.
(44) Lee, G.; Li, Y. C.; Kim, J.-Y.; Peng, T.; Nam, D.-H.; Rasouli, A. S.; Li, F.; Luo, M.; Ip, A. H.; Joo, Y.-C.; Sargent, E. H. Electrochemical Upgrade of CO 2 from Amine Capture Solution. *Nature Energy* **2020**, *6* (1), 46–53.
(45) Zhang, S.; Chen, C.; Li, K.; Yu, H.; Li, F. Materials and System Design for Direct Electrochemical CO2 Conversion in Capture Media. *J. Mater. Chem. A Mater. Energy Sustain.* **2021**. https://doi.org/10.1039/D1TA02751D.
(46) Jung, B.; Park, S.; Lim, C.; Lee, W. H.; Lim, Y.; Na, J.; Lee, C.-J.; Oh, H.-S.; Lee, U. Design Methodology for Mass Transfer-Enhanced Large-Scale Electrochemical Reactor for CO2 Reduction. *Chem. Eng. J.* **2021**, *424*, 130265.
(47) Liu, P. S. A New Method for Calculating the Specific Surface Area of Porous Metal Foams. *Philos. Mag. Lett.* **2010**, *90* (6), 447–453.
(48) Bui, J. C.; Digdaya, I.; Xiang, C.; Bell, A. T.; Weber, A. Z. Understanding Multi-Ion Transport Mechanisms in Bipolar Membranes. *ACS Appl. Mater. Interfaces* **2020**, *12* (47), 52509–52526.
(49) Knehr, K. W.; Agar, E.; Dennison, C. R.; Kalidindi, A. R.; Kumbur, E. C. A Transient Vanadium Flow Battery Model Incorporating Vanadium Crossover and Water Transport through the Membrane. *J. Electrochem. Soc.* **2012**, *159* (9), A1446.
(50) Campbell, F. W.; Belding, S. R.; Baron, R.; Xiao, L.; Compton, R. G. The Hydrogen Evolution Reaction at a Silver Nanoparticle Array and a Silver Macroelectrode Compared: Changed Electrode Kinetics between the Macro- and Nanoscales. *J. Phys. Chem. C* **2009**, *113* (33), 14852–14857.
(51) Krishtalik, L. I. *Charge Transfer Reactions in Electrochemical and Chemical Processes*; Springer Science & Business Media, 2012.
(52) Min, X.; Kanan, M. W. Pd-Catalyzed Electrohydrogenation of Carbon Dioxide to Formate: High Mass Activity at Low Overpotential and Identification of the Deactivation Pathway. *J. Am. Chem. Soc.* **2015**, *137* (14), 4701–4708.
(53) Seifitokaldani, A.; Gabardo, C. M.; Burdyny, T.; Dinh, C.-T.; Edwards, J. P.; Kibria, M. G.;

Bushuyev, O. S.; Kelley, S. O.; Sinton, D.; Sargent, E. H. Hydronium-Induced Switching between CO2 Electroreduction Pathways. *J. Am. Chem. Soc.* **2018**, *140* (11), 3833–3837.
(54) Mafé, S.; Ramírez, P.; Alcaraz, A. Electric Field-Assisted Proton Transfer and Water Dissociation at the Junction of a Fixed-Charge Bipolar Membrane. *Chem. Phys. Lett.* **1998**, *294* (4), 406–412.
(55) Mafé, S.; Ramírez, P. *Acta Polym.* **1997**, *48* (7), 234–250.
(56) McDonald, M. B.; Ardo, S.; Lewis, N. S.; Freund, M. S. Use of Bipolar Membranes for Maintaining Steady-State pH Gradients in Membrane-Supported, Solar-Driven Water Splitting. *ChemSusChem* **2014**, *7* (11), 3021–3027.
(57) McDonald, M. B.; Freund, M. S.; Hammond, P. T. Catalytic, Conductive Bipolar Membrane Interfaces through Layer-by-Layer Deposition for the Design of Membrane-Integrated Artificial Photosynthesis Systems. *ChemSusChem* **2017**, *10* (22), 4599–4609.
(58) McDonald, M. B.; Bruce, J. P.; McEleney, K.; Freund, M. S. Reduced Graphene Oxide Bipolar Membranes for Integrated Solar Water Splitting in Optimal pH. *ChemSusChem* **2015**, *8* (16), 2645–2654.
(59) Oener, S. Z.; Foster, M. J.; Boettcher, S. W. Accelerating Water Dissociation in Bipolar Membranes and for Electrocatalysis. *Science* **2020**, *369* (6507), 1099–1103.
(60) Shen, C.; Wycisk, R.; Pintauro, P. N. High Performance Electrospun Bipolar Membrane with a 3D Junction. *Energy Environ. Sci.* **2017**, *10* (6), 1435–1442.
(61) Mareev, S. A.; Evdochenko, E.; Wessling, M.; Kozaderova, O. A.; Niftaliev, S. I.; Pismenskaya, N. D.; Nikonenko, V. V. A Comprehensive Mathematical Model of Water Splitting in Bipolar Membranes: Impact of the Spatial Distribution of Fixed Charges and Catalyst at Bipolar Junction. *J. Memb. Sci.* **2020**, *603*, 118010.
(62) Blommaert, M. A.; Verdonk, J. A. H.; Blommaert, H. C. B.; Smith, W. A.; Vermaas, D. A. Reduced Ion Crossover in Bipolar Membrane Electrolysis via Increased Current Density, Molecular Size, and Valence. *ACS Appl. Energy Mater.* **2020**, *3* (6), 5804–5812.
(63) Nishida, K.; Murakami, T.; Tsushima, S.; Hirai, S. Measurement of Liquid Water Content in Cathode Gas Diffusion Electrode of Polymer Electrolyte Fuel Cell. *J. Power Sources* **2010**, *195* (11), 3365–3373.
(64) Angulo, A.; van der Linde, P.; Gardeniers, H.; Modestino, M.; Fernández Rivas, D. Influence of Bubbles on the Energy Conversion Efficiency of Electrochemical Reactors. *Joule* **2020**, *4* (3), 555–579.
(65) Nesbitt, N. T.; Burdyny, T.; Simonson, H.; Salvatore, D.; Bohra, D.; Kas, R.; Smith, W. A. Liquid–solid Boundaries Dominate Activity of CO2 Reduction on Gas-Diffusion Electrodes. *ACS Catal.* **2020**, *10* (23), 14093–14106.
(66) Jähne, B.; Heinz, G.; Dietrich, W. Measurement of the Diffusion Coefficients of Sparingly Soluble Gases in Water. *J. Geophys. Res.* **1987**, *92* (C10), 10767.
(67) Zenyuk, I. V.; Medici, E.; Allen, J.; Weber, A. Z. Coupling Continuum and Pore-Network Models for Polymer-Electrolyte Fuel Cells. *Int. J. Hydrogen Energy* **2015**, *40* (46), 16831–16845.
(68) Weber, A. Z.; Newman, J. Modeling Transport in Polymer-Electrolyte Fuel Cells. *Chem. Rev.* **2004**, *104* (10), 4679–4726.
(69) Zhang, Z.; Melo, L.; Jansonius, R. P.; Habibzadeh, F.; Grant, E. R.; Berlinguette, C. P. pH Matters When Reducing CO2 in an Electrochemical Flow Cell. *ACS Energy Lett.* **2020**, *5* (10), 3101–3107.
(70) Vermaas, D. A.; Wiegman, S.; Nagaki, T.; Smith, W. A. Ion Transport Mechanisms in Bipolar Membranes for (photo)electrochemical Water Splitting. *Sustainable Energy Fuels* **2018**, *2* (9), 2006–2015.
(71) Grew, K. N.; Chiu, W. K. S. A Dusty Fluid Model for Predicting Hydroxyl Anion Conductivity in Alkaline Anion Exchange Membranes. *J. Electrochem. Soc.* **2010**, *157* (3), B327.
(72) Wang, X.; Van Nguyen, T.; Hussey, D. S.; Jacobson, D. L. An Experimental Study of Relative

Permeability of Porous Media Used in Proton Exchange Membrane Fuel Cells. *J. Electrochem. Soc.* **2010**, *157* (12), B1777.
(73) Zhang, Z.; Lees, E. W.; Habibzadeh, F.; Salvatore, D. A.; Ren, S.; Simpson, G.; Liu, D. W. A.; Berlinguette, C. P. Metallic Porous Electrodes Enable Efficient Electrolysis of Liquid CO2 Capture Solutions.
(74) Todinca, T.; Tănasie, C.; Pröll, T.; Cătа, A. Absorption with Chemical Reaction: Evaluation of Rate Promoters Effect on CO2 Absorption in Hot Potassium Carbonate Solutions. In *Computer Aided Chemical Engineering*; Pleşu, V., Agachi, P. Ş., Eds.; Elsevier, 2007; Vol. 24, pp 1065–1070.
(75) Thee, H.; Suryaputradinata, Y. A.; Mumford, K. A.; Smith, K. H.; Silva, G. da; Kentish, S. E.; Stevens, G. W. A Kinetic and Process Modeling Study of CO2 Capture with MEA-Promoted Potassium Carbonate Solutions. *Chem. Eng. J.* **2012**, *210*, 271–279.
(76) Rochelle, G. T.; Sexton, A.; Davis, J.; Hilliard, M.; Xu, Q.; Van Wagener, D.; Plaza, J. M. *CO2 Capture by Absorption with Potassium Carbonate*; University Of Texas At Austin, 2007.
(77) Zhu, S.; Jiang, B.; Cai, W.-B.; Shao, M. Direct Observation on Reaction Intermediates and the Role of Bicarbonate Anions in CO2 Electrochemical Reduction Reaction on Cu Surfaces. *J. Am. Chem. Soc.* **2017**, *139* (44), 15664–15667.
(78) Dunwell, M.; Lu, Q.; Heyes, J. M.; Rosen, J.; Chen, J. G.; Yan, Y.; Jiao, F.; Xu, B. The Central Role of Bicarbonate in the Electrochemical Reduction of Carbon Dioxide on Gold. *J. Am. Chem. Soc.* **2017**, *139* (10), 3774–3783.
(79) Yan, Z.; Hitt, J. L.; Zeng, Z.; Hickner, M. A.; Mallouk, T. E. Improving the Efficiency of CO2 Electrolysis by Using a Bipolar Membrane with a Weak-Acid Cation Exchange Layer. *Nat. Chem.* **2021**, *13* (1), 33–40.
(80) Zhang, Z.; Sadeghi, M. A.; Jervis, R.; Ye, S.; Gostick, J. T.; Barralet, J. E.; Merle, G. Tailoring Carbon Nanotube Microsphere Architectures with Controlled Porosity. *Adv. Funct. Mater.* **2019**, *29* (42), 1903983.
(81) Li, D.; Wu, J.; Liu, T.; Liu, J.; Yan, Z.; Zhen, L.; Feng, Y. Tuning the Pore Structure of Porous Tin Foam Electrodes for Enhanced Electrochemical Reduction of Carbon Dioxide to Formate. *Chem. Eng. J.* **2019**, *375*, 122024.
(82) Vorhauer, N.; Altaf, H.; Tsotsas, E.; Vidakovic-Koch, T. Pore Network Simulation of Gas-Liquid Distribution in Porous Transport Layers. *Processes* **2019**, *7* (9), 558.
(83) Zenyuk, I. V. Bridging X-Ray Computed Tomography and Computational Modeling for Electrochemical Energy-Conversion and –storage. *Curr. Opin. Electrochem.* **2019**, *13*, 78–85.

For Table of Contents only